Mechanical Cloaking of Cutouts in Laminated Plates

Calum J. McInnes*, Alberto Pirrera†, Byung Chul Kim‡, and Rainer M. J. Groh§
Bristol Composites Institute,
Queen's Building, University Walk, Bristol, BS8 1TR, UK

The presence of a central cutout in thin, plate-like structures often results in a reduction in load-carrying capacity due to a removal of bending stiffness at the unsupported central region. This paper presents a design approach that minimizes the mechanically detrimental effect of a central circular cutout on the buckling performance of a flat, square, simply supported plate under uniaxial compression, for a hole diameter-to-plate-width ratio of $D/l_y = 0.3$. We consider the potential design of a holed laminated plate to have the performance of an unholed target design by application of the variable-angle Continuous Tow Shearing (CTS) process to generate periodic stiffness variations, in order to significantly disrupt and redirect prebuckling stresses. Parallelized population-based optimization approaches are used to find structural solutions which can meet the target unholed plate performance with lowest mass increase. Both holed straight fiber and fiber-steered designs are found which give near-identical structural performance to an optimum unholed eight-ply straight fiber plate of square aspect ratio ($[\pm 45]_{2s}$). The holed eight-ply straight fiber plate gives near identical prebuckling stiffness and within $\pm 3\%$ buckling load of the holed plate for a 21% mass increase where ply-level orientations ($[\pm 79/\pm 54]_s$) and ply-level thicknesses ($[(1.22t_0)_2/(1.37t_0)_2]_s$) are allowed to vary. Comparatively, the eight-ply holed CTS fiber-steered plate ($[\pm 90\langle 33|21\rangle^{10}/\pm 90\langle 52|2\rangle^4]_s$) achieves within 1% of the prebuckling stiffness and $\pm 1\%$ of the buckling load of the target unholed plate for a 9% mass increase. Stress analysis is conducted to identify the governing mechanics that account for the improved performance of the CTS fiber steered plate. We find that the fiber-steered solution removes high-magnitude stresses away from the hole boundary to a region of higher stiffness within the plate, which are produced by the fiber angle-ply thickness coupling of the CTS process. Overall, the findings of the present work indicate a suitable direction for future research and the need to further investigate the non-intuitive mechanics arising from CTS fiber steering for application to future aerostructural research and development.

Nomenclature

A_{ij}	=	Elements from extensional stiffness matrix $[A]$
d^i	=	Half-period length of i^{th} ply
D	=	Hole diameter
$\overline{E}_x$	=	Equivalent prebuckling stiffness
f_i	=	Scaling factor applied to i^{th} ply
l_x, l_y	=	Length of plate in x- and y-directions respectively
m	=	Structural mass
N	=	Number of plies in laminate
n^i	=	Shearing periodicity of i^{th} ply
P_{cr}	=	Critical buckling load
r_s	=	Steering radius of CTS process
T_0^i	=	Mid-period fiber reference path angle of i^{th} ply, taken clockwise from ϕ
T_1^i	=	Ending fiber reference path angle of i^{th} ply, taken clockwise from ϕ

*PhD Student, Bristol Composites Institute, University of Bristol, UK
†Professor of Nonlinear Structural Mechanics, Bristol Composites Institute, University of Bristol, UK
‡Associate Professor in Composites Design and Manufacture, Bristol Composites Institute, University of Bristol, UK
§Lecturer in Digital Engineering of Structures, Bristol Composites Institute, University of Bristol, UK

t_0, t = Tow thickness of a ply pre- and post-shearing, respectively
x' = One dimensional position along steering line
α = Orthotropy ratio
θ^i = Local fiber angle, of i^{th} ply, taken from global x-axis
ϕ^i = Angle from global x-axis of part which denotes unsheared direction of i^{th} ply
ϕ_d = Angle required for diagonal bisection of ply

I. Introduction

The presence of holes in plates is a long-standing problem in structural mechanics due to their complicating effects on structural response under loading [1]. Holes, or more colloquially, cutouts, are typically associated with a resulting decrease in plate compression buckling performance [2]. By removing material from the plate center, a loss in bending stiffness is caused. This bending stiffness loss can reduce the load-carrying capacity of the plate if the prebuckling axial load path is also centrally located [2]. For isotropic plates, alignment of the mechanical load paths with the central cutout is typical. Further complicating, often compounding, mechanical effects are encountered when material anisotropy is introduced, which results in orthogonally differing stiffness values across the structure. In general, the problem of a central cutout in plates is of importance in aerostructural design as cutouts are often used as standard features in air- and spacecraft to allow inspection holes, fuel line routing or fastener locations [2]. Plates are typical components in sub-assemblies such as wing web spars, as an example. Early work on plates with central cutouts under compression loading was conducted by Nemeth [3], who compared analytical expressions for the postbuckling response of simply supported square plates under stress loading against experimental studies to good agreement for hole sizes up to diameter, D, to width, l_y, ratios of $D/l_y = 0.5$. Marshall *et al.* obtained analytical solutions for the buckling of displacement loaded, simply supported plates using the Rayleigh-Ritz method that showed good agreement up to hole diameter to plate width ratios up to $D/l_y \leq 0.7$, with excellent agreement with experiments up to $D/l_y \leq 0.5$ [4]. In addition, the work of Lee *et al.* [4] began to show the effects of cut-out size, material orthotropy and plate aspect ratio on the buckling behavior of simply supported plates. Prebuckling membrane stress distributions were subsequently studied by Nemeth [3].

In 1991, Hyer and Lee presented the use of curvilinear fiber orientations [5], which is herein referred to as fiber steering, to improve the buckling resistance of a square simply supported plate with a central cutout [6]. This investigation made the case for increasing buckling performance of laminated plates by the fiber steering concept to tailor the prebuckling near- and far-field stress fields [7]. Jegley *et al.* conducted experiments on variable stiffness flat plates under axial compression or shear [7]. The buckling, postbuckling and failure behavior of elastically tailored plates was studied to experimentally show that buckling performance improvements are attainable by fiber steering for plates with central circular cutouts [7]. Lopes *et al.* subsequently investigated the potential for designing fiber-steered plates such that the buckling and failure response are insensitive to the existence of a central hole [8]. This near structural insensitivity to material removal is one of the motivating ideas of the present work. Lopes *et al.* found that redistribution of loading towards the supported edges resulted in a performance benefit by unloading the central section [8]. Lopes *et al.* noted that both the critical buckling load and structural stiffness of fiber-steered plates are unaffected by the presence of a central hole on a square plate [8]. Lopes *et al.*'s conclusion of prebuckling load redistribution towards edge supports matches that found for plates without cutouts by Gürdal *et al.* [9]. Thus, fiber-steered structural research studies have included the presence of cutouts in design studies. Recently, Zucco *et al.* investigated the potential of steering around a central elliptical cutout to achieve an increase in buckling performance when compared to an equivalent straight fiber plate [10]. Zucco *et al.* [10] reported a 26% increase in buckling load for a 17% plate mass increase. Moreover, the method for steering material tows around a central elliptical cutout always results in a resin-rich area in close vicinity to the cutout in the direction of steering. Comparatively, the presence of cutouts in structures is analogous to a problem found in nature, where cellulose fibers in wood grow in helical trajectories around a knot [11]. Thus, in natural fibrous materials, the fibers do not terminate at the knot boundaries but instead follow curved paths as to reduce stress concentrations by means of a stiffness gradient. Hence, if this analogy is applied to structural design one can expect to find improved performance by taking inspiration from the natural world.

To date, when manufacturing fiber-steered demonstrator structures, such as that for an air-launch-to-orbit system by NASA, studies have commonly steered material tows by the Automated Fiber Placement (AFP) process [12]. However, due to the inherent material deformation mechanism a susceptibility to defects is inherent in AFP [13]. AFP steers

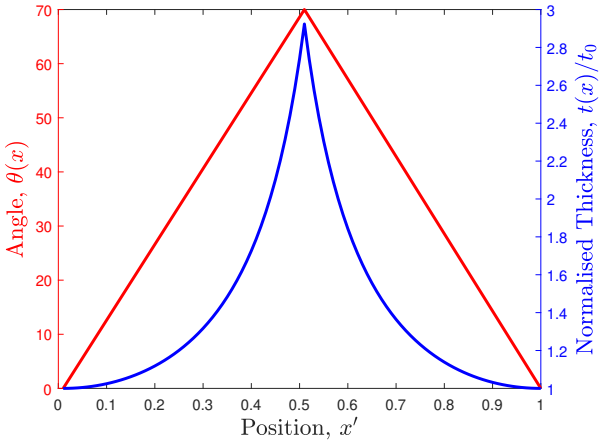

Fig. 1 Nonlinearity of mechanical orientation-thickness coupling when fiber steering by CTS process pre- and post-shearing for a $\langle 0|T_1\rangle$ tow-steered ply of linear angle variation by CTS. Note this particular variation in fiber angle can give rise to a maximum potential mass increase of $1.42\times$. The maximum potential mass increase of a CTS structure is found for a $\langle 70|70\rangle$ which would cause a $3\times$ increase.

material tows by in-plane bending [14], which leads to tow wrinkling and bridging, which can be associated with a decrease in structural performance [15] and increase in both analytical and numerical analysis complexity. Moreover when bending material tows an inability to tessellate occurs, leading to the need for either gaps or overlaps in an AFP tow-steered ply [16]. To avoid such process-inherent limitations, the Continuous Tow Shearing (CTS) process was developed by Kim *et al.* [14]. The CTS process instead shears material tows in-plane to fiber steer. By shearing tows in-plane, tessellation is possible and hence a ply can be fully covered without the need for gaps or overlaps, leading to a simplification of both the geometric discretization and computational analysis [17]. This in-plane shearing mechanism used by the CTS process gives rise to a mechanically nonlinear fiber orientation-ply thickness coupling, where due to material volume conservation pre- and post-shearing, a thickness change occurs [14]. This nonlinear orientation-thickness coupling is expressed, for a one-dimensional variation along the x'-axis, the one-dimensional position along the steering line, as

$$t(x') = t_0 \sec(\theta(x')) \tag{1}$$

where t and t_0 are the pre- and post-shearing thickness of a material tow, respectively, and θ is the change in fiber angle compared to the unsheared direction. The nonlinearity to this mechanical coupling is visualized in Fig.1.

In their early work Kim *et al.* [18] produced models of CTS plates with central cutouts. However, no structural analysis was pursued, possibly due to the novelty of the manufacturing process and subsequent focus on technological maturation. Groh and Weaver utilized the CTS process to conduct a mass-optimization study of laminated plates using a population-based optimization approach [19]. It was reported that a 31% mass reduction is achievable when meeting both failure and buckling constraints of a rectangular plate when compared to a conventional straight fiber baseline design. Groh and Weaver also investigated the postbuckling stability of their optimized designs found by their Genetic Algorithm optimizer. Several of the CTS layups presented by Groh and Weaver exhibited stiffer postbuckling behavior than the straight fiber baseline design, which was selected as Quasi-Isotropic. Finally, Groh and Weaver also commented on the potential of the CTS process to achieve both global and local stiffness tailoring to alter the buckling performance of laminated plates by positioning of stiffness at critical regions on the plates.

The remainder of the paper is structured as follows. Section II outlines the motivation for the current work and the working hypothesis of the investigations. Section III summarizes a useful model for uniaxial compression buckling of simply-supported orthotropic plates. Section IV outlines the significant effort required in the formulation of Finite Element models of holed CTS fiber-steered plates. Two optimization problems are presented in Section VI, one straight fiber and one fiber-steered as to ascertain the mass increase associated with mechanical cloaking by both structure types. Results are presented in Section VII and the results are discussed. Finally, conclusions are made in Section VIII.

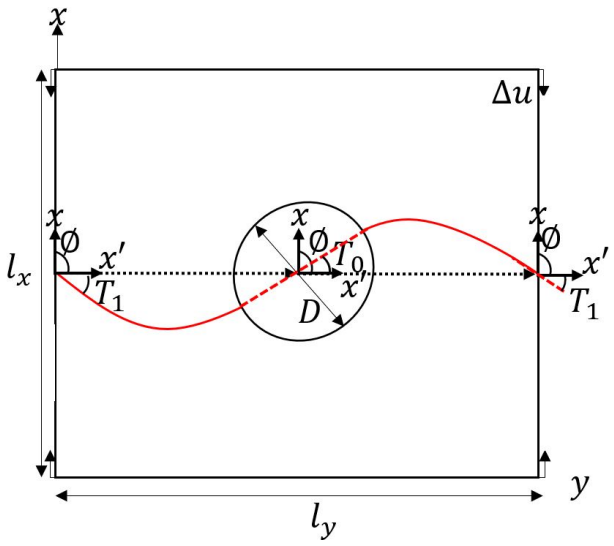

Fig. 2 Steering notation employed in this work. ϕ is the angle between the global $x-$axis and local x'-axis, where due to $\phi = 90$ in this particular reference path the x'-axis is aligned with x. T_1 is the angle from x' at the beginning of a shearing period. Similarly T_0 is the angle from x' at the mid-period. Note fibers are not steered explicitly around the central hole instead they terminate at the boundary. This is equivalent to hole creation on the plate post material layup. N.B. fiber path presented here is for illustrative purposes only.

A. CTS Tow Steering Notation

Prior to further investigation and presentation, it is pertinent to first define the notation employed in this work for fiber-steered reference path design. The notation used for CTS fiber-steered structural design in this work follows that of Gürdal *et al.* [20], whereby 2 control points, T_0 and T_1 are equally spaced on a period of half-length d at an orientation ϕ to the plate $x-$axis. Positional fiber angles vary both linearly and symmetrically about T_0 at the period center to T_1 at the period edges, in accordance with Gürdal *et al's.* notation [20]. Due to the smaller steering radius achievable by the CTS process compared to AFP the potential for multiple steering periods is permissible, whereby the linear variation of $T_1 \rightarrow T_0 \rightarrow T_1$ is repeated n times along the ϕ direction. We assume that the periods are equally spaced and thus the resulting thickness build-ups have equal pitch. Hence, a single CTS tow-steered ply, of periodic linear fiber angle variation is expressed simply through addition of a superscript n as

$$\phi\langle T_0|T_1\rangle^n. \tag{2}$$

An example of this notation is visualized in Fig.2 which denotes an arbitrary $\phi\langle T_0|T_1\rangle^n$ variation. Furthermore, in this work fiber angles vary linearly along the x'-axis, which is simply an axis rotated by ϕ from the part x-axis, as

$$\theta(x') = \phi + \frac{(T_1 - T_0)}{d}|x'| + T_0. \tag{3}$$

B. Mass Dependence

As discussed previously, the nonlinear orientation-thickness coupling gives rise to a mass increase when fiber steering by the CTS process. For an unholed CTS fiber-steered structure, the normalized mass increase of a CTS fiber-steered structure as a function of end-period angle, assuming $T_0 = 0°$ is plotted in Fig. 1. As can be observed in Fig. 1 when shearing material tows by the maximum allowed value a CTS structure can exhibit a 42% mass increase when steering linearly from 0° to 70°.

II. Motivation

The potential for increasing the performance of holed laminated plates by fiber steering has been investigated by a number of studies [7, 8, 10]. However, the concept of altogether cloaking, masking or concealing the mechanical effects

of cutouts on laminated plates by the fiber steering concept has received little attention. The idea of mechanical cloaking has received investigation from the field of metamaterials by material design to directly influence the elastic response of loaded structures, which has been investigated by Wang *et al.* [21]. Wang *et al.*'s method concurrently optimized the topology and properties to produce aperodic structural cloaking configurations for several boundary conditions [21]. Wang *et al.*'s design configuration, for a plate with central circular hole under displacement loading, achieved a 4% difference in directional spatial displacement fields when cloaked, compared to 17.2% when uncloaked [21]. Optimization-based design by Fachinotti *et al.* [22] presented a device to manipulate displacement fields on a structure under uniaxial compression loading. Fachinotti *et al.* plotted displacement fields for both homogeneous plates and plates with a cloaked hole. These displacement fields, in both horizontal and vertical directions indicate that one can design a device such that the displacements magnitudes of a cloaked hole are equal to that of a homogeneous baseline, with close correlation in spatial fields [22]. Furthermore, Bückmann *et al.* [23] presented the cloaking of a void in an elastic material under static uniaxial compression. Bückmann *et al.'s* work discussed the demanding nature of the problem and presented both numerical and experimental results. Bückmann *et al.* quantified cloaking quality by comparing average relative standard deviation of strain vectors on the cloaked material with reference to a homogeneous baseline. Overall, Bückmann *et al.'s* hypothesis is that intelligent material design can allow for stress peaks to be separated from hole boundaries and redistributed on a structural domain. This notion of stress redistribution is the current working hypothesis of the fiber-steered composites literature. In the case of plate compression buckling, prebuckling stresses are redistributed from the plate center towards the supported edges leading to increased structural performance [24]. Hence, one can expect there to be a commonality in the underlying mechanics between fiber-steering and metamaterial design. For example, Fachinotti *et al.* achieved mechanical cloaking by positioning higher stiffness material around a hole on a Nylon plate [22].

It is the hypothesis of this work that instead of substituting higher stiffness isotropic material at locations on the structure, an equivalent means of stiffness distributions are achieved by fiber steering of laminated composites. By fiber steering, the stiffness distributions are generated across a structure during material deposition. The existing literature has demonstrated that fiber-steered composites are an ideal method for designing variable stiffness structures due to the inherent material anisotropy of fiber-reinforced composite material systems.

III. Theory

In the stability analysis of orthotropic plates under uniaxial compression Stein calculated a second-order solution to von-Karman's isotropic plate equations [25]. This analysis is extended by Chandra and Raju to plates comprising of orthotropic materials [26]. From White [27] the critical buckling eigenvalue of a simply supported unholed rectangular orthotropic plate is

$$P_{\text{cr}} = \frac{\pi^2 h^3}{12 l_x^2 l_y^3 m^2 (\alpha - \nu_{yx}^2)} (E_x \alpha^2 l_x^4 n^4 + E_x \alpha l_y^4 m^4 + \{2 E_x \alpha \nu_{yx} + 4 G_{xy} (\alpha - \nu_{yx}^2)\} l_x^2 l_y^2 m^2 n^2), \tag{4}$$

where one must iteratively check the eigenmode in which the critical buckling eigenvalue occurs by successive substitution of buckled mode shapes, which are here defined by n, m, the number of half-waves in the x- and y-directions, respectively, of a buckled structural mode shape. The orthotropy ratio, α, of a particular material system is found by $\frac{E_y}{E_x}$. Moreover, from Weaver [28] and Nettles [29] the effective in-plane engineering constants of an orthotropic layup are found from the extensional stiffness matrix terms A_{ij}, as

$$E_x = \frac{1}{h}\left(\frac{A_{11}A_{22} - A_{12}^2}{A_{22}}\right), \quad E_y = \frac{1}{h}\left(\frac{A_{11}A_{22} - A_{12}^2}{A_{11}}\right), \quad G_{xy} = \frac{1}{h}, \quad \nu_{xy} = \frac{A_{12}}{A_{22}}, \quad \nu_{yx} = \frac{\left(\frac{A_{16}A_{26}}{A_{66}} - A_{12}\right)}{\left(\frac{A_{16}^2}{A_{66}} - A_{11}\right)}. \tag{5}$$

Thus, from this analytical formulation it is of low computational cost to find the buckling load of simply supported unholed othrotropic plates when knowing both geometry and material properties. This formulation is used for verification of Finite Element models.

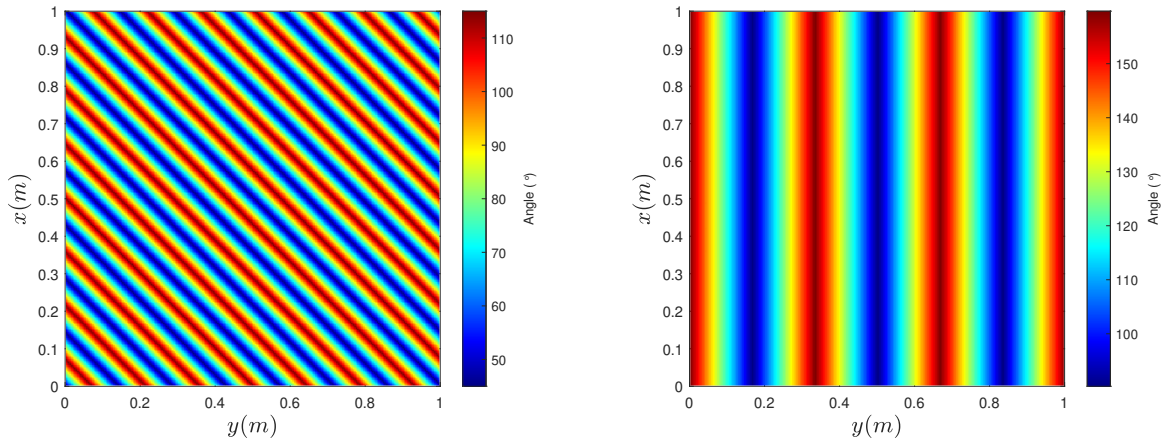

Fig. 3 Examples of fiber orientation distributions arising from steering directions considered in this work (L) $\phi = 45°$, (C) $\phi = 90°$ on unholed CTS fiber-steered plates of aspect ratio $l_x/l_y = 1$. Each steering direction has differing example steering periodicity (L) $n = 5$, and (R) $n = 14$. Note the number of periods is counted from the plate center outwards along the steering direction, hence, for odd periodicities such as that in (L) and (R) one will count half periods at the plate edges.

IV. Geometry

Gürdal's notation [20] for a linear variation in fiber angle first requires computation of the half-period length of the k^{th} ply, d^k, which for a plate of length l_x and width l_y in the global x- and y-directions, respectively, is derived as

$$d^k = \begin{cases} l_x \left(\cos\phi^k + \frac{\sin^2\phi^k}{\cos\phi^k} \right), & \text{if } 0° \leq \phi^k \leq \phi_d \\ \\ l_y \left(\sin\phi^k + \frac{\cos^2\phi^k}{\sin\phi^k} \right), & \text{if } \phi_d < \phi^k \leq 90° \end{cases}, \tag{6}$$

where the angle required for formulation of a diagonal bisection of the plate, ϕ_d, is

$$\phi_d = \sin^{-1}\left(\frac{l_y}{\sqrt{l_x^2 + l_y^2}} \right). \tag{7}$$

As the in-plane dimensions are held constant between plies this angle holds for all plies. One will observe that if $\phi^k = 0°$ the length of the half-period line, d^k, simplifies to half the plate's x-direction dimension. Similarly, if $\phi^k = 90°$ the length of the steering line is simply half the length of the plate in the y-direction. Likewise, if $\phi^k = 45°$ the length of the steering line is equal to the length of the diagonal bisection line, $\sqrt{l_x^2 + l_y^2}$. Many prior studies have considered $\phi^k = [0°, 90°]$ steering directions for formulation of a manageable design space [30–33]. Furthermore, this choice of $\phi^k = [0°, 90°]$ is that in which Gürdal *et al.* identified as promising configurations in load path redistribution through structural stiffness tailoring [20]. Moreover, previous work identified the choice of $\phi^k = 0°$ or $\phi^k = 90°$ to allow for relatively simple and efficient numerical discretization strategies to be employed [17]. Examples of several steering directions, periodicities and their resulting fiber orientation distributions are presented in Fig. 3 for an unholed square aspect ratio CTS fiber-steered plate for clarity.

The fiber angle distributions occurring from fiber steering vary along the x'-direction and are tessellated/shifted perpendicular to this axis. Note that when $\phi^k \neq 0°$ the x'-direction is rotated by ϕ^k from the x-axis. Thus, one can fully cover the planform of a ply without the need for either gaps or overlaps such as that required when fiber steering by AFP.

Herein the ply-level periodicity (n^k) denotes the number of shearing periods per ply and thus the following conditional is formulated as to ascertain the maximum number of thickness build-ups allowable per ply, which is directly dependent

Table 1 Material properties of IM7/8552, reproduced from [27]

E_1 (GPa)	E_2 (GPa)	G_{12} (GPa)	G_{13} (GPa)	ν_{12}	G_{23} (GPa)	ρ (kg/m^3)	t_0 (mm)
163	10	5	5	0.333	6.0023	1570	0.131

upon its steering direction as

$$\max(n^k) = \begin{cases} \frac{2l_x r_s}{\cos(\phi^k)}, \text{if } \phi^k \leq \tan^{-1}\left(\frac{l_x}{l_y}\right) \\ \\ \frac{2l_y r_s}{\sin(\phi^k)}, \text{if } \phi^k > \tan^{-1}\left(\frac{l_x}{l_y}\right) \end{cases}, \tag{8}$$

where the resulting maximum number of thickness build-ups given by Eqn. 8 is rounded down to the nearest integer value. Downwards rounding is used such that the manufacturing constraint is never violated and as such an integer number of shearing periods is considered. Finally, the accompanying thickness distributions arising from a particular fiber angle distribution are relatively simple to compute and are done so by simply extending Eqn. 1 to

$$t^k(x, y) = t_0 \sec(\theta^k(x, y) - \phi^k). \tag{9}$$

V. Finite Element Model

This work uses the commercially available finite element solver Abaqus [34] to investigate the structural performance of CTS fiber-steered plates. Plates without a central hole are meshed by 2 layers of 8-noded continuum shell elements (SC8R) within an automated MATLAB [35] mesh generator. Geometrical discretization is achieved by linearly spaced in-plane points and 3 layers of nodes out-of-plane. The choice of 8-noded continuum shell elements is made as to allow for application of loading and support conditions directly to the mid-plane of the plate. The greater geometrical fidelity of solid-shell elements is additionally important as it allows for straightforward modelling of a curved top surface and a flat bottom surface, as is typically the case in CTS panels cured on a flat tool plate. The continuum/solid shell elements, due to their non-prismatic cross section can approximate the asymmetric curvature more accurately than equivalent single layer shells, without having to employ full brick elements, which are of considerable computational expense. Loading is introduced as a uniform end-shortening and plate boundary conditions are set to disallow out-of-plane translation, *i.e.* $w = 0$ at all edges of the plate.

Furthermore, when seeking to discretize CTS fiber-steered plates a further consideration of desirable node location must be made to allow for accurate modeling of the geometry. In order to accurately represent the variable thickness geometry of CTS plates a robust meshing strategy is devised. By creating Abaqus geometrical models using the Python scripting interface, partitions are created to locate nodes at expected locations of thickness maxima. The Python tool automatically creates the plate, partitions the geometry along lines of thickness maxima, seeds nodes both in-plane and through-thickness and meshes the part. An input (.inp) file is created which lists both nodal locations and element connectivities, all that is required for passing to a custom MATLAB fiber steering algorithm. This algorithm considers node- and element-wise coordinates relative to a steering period's center in order to compute both angle and thickness variations. Angle values are computed at nodes and element centroids, where an arbitrary i^{th} 8-noded element's centroid (x_c^i, y_c^i, z_c^i) is found by geometrical averaging as,

$$(x_c^i, y_c^i, z_c^i) = \frac{1}{8}\sum_{j=1}^{8}(x_j^i, y_j^i, z_j^i). \tag{10}$$

Angles computed at nodes are required to operate on the automated Python-generated mesh and redefine the through-thickness, z-coordinate due to the thickness variations generated by CTS fiber steering. Furthermore, loading and boundary conditions are applied to nodes residing at both mid-thickness plate edge nodes, as discussed prior. Finally, the pristine (unsheared) material used in this work is a typical aerospace-grade advanced composite material system, IM7/8552, with properties presented in Tab. 1.

Prior to any optimization a multi-parameter numerical convergence study, where end-shortening eigenvalue, buckling load and effective stiffness are measured for successively finer meshing resolutions, is conducted on a plate with largest shearing angle ($T_0^1 = T_0^2 = 0°$, $T_1^1 = T_1^2 = 70°$) and shearing direction set to $\phi^1 = \phi^2 = 90°$. A linear perturbation

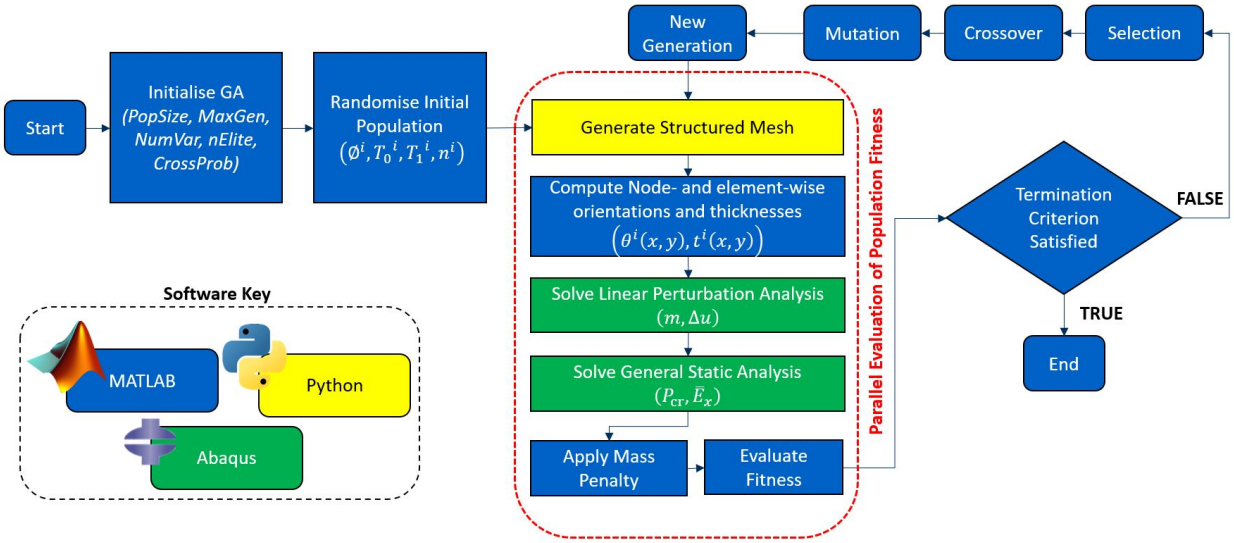

Fig. 4 Full computational optimization flowchart for CTS fiber-steered problem. Note the use of parallelization in evaluation of a generation's population fitness function. This is possible due to the non-gradient basis of GAs.

analysis is employed to find the end-shortening eigenvalue required to initiate buckling. This eigenvalue is then passed to a general static analysis to find the critical buckling load of the configuration by summation of corresponding reaction forces along the loaded nodes. Due to the variation in fiber angle perpendicular to the loading direction, a non-constant stiffness is present along the loaded edge and thus a non-constant reaction force is generated. Equivalent structural stiffness is found following the linear prebuckling assumption of the linear perturbation analysis and, by extension, Hooke's law. Numerical convergence of the model is deemed to have been achieved when the difference between recorded results iterations is less than 1%. This convergence study resulted in an minimum required mesh resolution of 72, 158 SC8R elements, corresponding to 398, 250 degrees of freedom. The use of the automated Python partitioning tool to place nodes at locations of thickness maxima results in relatively efficient geometric capture and structural discretization of the variable thickness profile of this particular periodically steered CTS plate.

VI. Optimization

The objective of this work is to find whether the mass increase associated with mechanically cloaking a central hole on a square plate is lower using CTS fiber steering than that obtained by employing common straight fiber laminates. Hence, the following subsections discuss and present problem statements for the two required optimizations to interrogate this hypothesis. Section VI.A presents the optimization for mechanical cloaking by either ply orientation or thickness alteration. Section VI.B presents the optimization for mechanical cloaking by generating fiber orientation and thickness distributions by CTS fiber steering. For all optimizations in this work a population based optimization algorithm is chosen due to its flexibility and applications to problems across disciplines [36]. The optimization problems presented in Sections VI.A and VI.B are solved using the GA function, for single objective problems in the global optimization toolbox in MATLAB. A feature of the global optimization toolbox is the ability to solve the optimization problems by use of parallel processing on a multicore processor. As GAs are population- not gradient-based the evaluation of a population's fitness can be conducted simultaneously in a generation. Overall, parallelization of a GA allows for significant time reductions by individual CPU cores evaluating the fitness function. When individual evaluations are computationally expensive, such as that found herein, the ability to parallelize is invaluable. For both optimizations the number of elite solutions is 2, the crossover fraction is 0.8, furthermore the population size is 50 and maximum number of generations are 30 to keep total optimization run times within 5 days. A visualization of the full computational optimization process is presented in Fig. 4 where the linking of different software (Matlab, Python and Abaqus) and handling of data for numerical model generation and fitness function evaluation is presented.

A. Mechanical Cloaking by Straight Fiber Laminates Formulation

Before considering fiber-steering this work ascertains the straight fiber design required to 'cloak' the presence of the central hole. We define a cloaked hole as one where the performance of the holed plate is equal to that of the unholed plate. The performance metrics chosen for this work are the common aerospace criteria for stability: critical buckling load and prebuckling stiffness. Hence, if the critical buckling load and prebuckling stiffness of a holed plate is equal to that of an unholed plate this is sufficient to satisfy cloaking in this work. Thus, to optimize a holed straight fiber plate for cloaking the following problem statement is formulated, where the euclidean distance between the current and target performance, in 2-dimensional space, is minimized as

$$\begin{aligned} \min_{x} \quad & \sqrt{(P_{\text{cr}}^{\text{SF,Hole}}(x) - P_{\text{cr}}^{\text{ref.}})^2 + (\overline{E}_{x,\text{pre}}^{\text{SF,Hole}}(x) - \overline{E}_{x,\text{pre}}^{\text{ref.}})^2} \\ \text{Variables:} \quad & x = [\theta_1, \theta_2, f_1, f_2] \\ \text{Subject to:} \quad & 0^\circ \leq \theta_i \leq 90^\circ (i = 1, 2) \\ & 1 \leq f_i \leq 1.5 (i = 1, 2) \end{aligned} \tag{11}$$

where f_i is the scaling factor applied to the i^{th} ply thickness of the layup which is set to be balanced and symmetric of the form $[\pm\theta_1/\pm\theta_2]_s$. The optimizer is assisted by selecting only positive fiber angles, as it is well known that stacking sequences of the form $[\pm\theta]_{NS}$ give highest buckling performance $\theta = 45^\circ$, in addition to stiffness $\theta = 0^\circ$. Furthermore the possible ply thickness increase is set to between 1 and 1.5 times the nominal ply thickness t_0, which is presented in Tab. 1. In structural optimization for lightweighting it is evidently important to include some form of penalty to solutions with high mass. It is possible by following the optimization formulation of Eqn. 11 that the optimizer may become entrapped in a region of the potential solution space that does meet the buckling and stiffness performance requirements yet with a high mass, which is evidently counter to that desired for lightweight structural solutions. Thus, Eqn.11 is extended into an additional dimension and rewritten using a penalty method applied to the mass of a solution as

$$\min_{x} \quad m(x) \cdot (1 + \sqrt{(P_{\text{cr}}^{\text{SF,Hole}}(x) - P_{\text{cr}}^{\text{ref.}})^2 + (\overline{E}_{x,\text{pre}}^{\text{SF,Hole}}(x) - \overline{E}_{x,\text{pre}}^{\text{ref.}})^2})^3 \tag{12}$$

where $m(x)$ is the mass of a solution. This additional dimension to the problem penalizes solutions with high mass and instead guides the optimizer to structures with equal performance to the target for the lowest associated mass increase. Here, solutions that meet the mechanical cloaking criterion with a high mass increase are penalized rather aggressively by selecting the penalty exponent as the cubic power.

B. Mechanical Cloaking by Fiber-Steered Laminates Formulation

It is the objective of this optimization to find a holed CTS fiber-steered plate with both equal buckling load and prebuckling stiffness to that of an unholed straight fiber plate. Due to the nonlinear orientation-thickness coupling of the CTS process there also exists a nonlinear orientation-mass coupling. As fibers are sheared in-plane the thickness, and thus mass, increases by material volume conservation. Where the mass increase of the straight fiber optimization presented prior in Section VI.A comes from increasing the overall thickness of the i^{th} ply in the balanced and symmetric layup, the mass increase of the CTS fiber-steered plate arises due to this non-linear mechanical coupling. Hence, in order to achieve a CTS layup which can mechanically cloak the presence of a central hole the resulting buckling load and prebuckling stiffness are compared to the reference panel in an identical method to that prior as

$$\begin{aligned} \min_{x} \quad & \sqrt{(P_{\text{cr}}^{\text{CTS, Hole}}(x) - P_{\text{cr}}^{\text{ref.}})^2 + (\overline{E}_{x,\text{pre}}^{\text{CTS, Hole}}(x) - \overline{E}_{x,\text{pre}}^{\text{ref.}})^2} \\ \text{Variables:} \quad & x = [\phi_1, T_{0,1}, T_{1,1}, n_1, \phi_2, T_{0,2}, T_{1,2}, n_2] \\ \text{Subject to:} \quad & 0^\circ \leq \phi_i \leq 90^\circ (i = 1, 2) \\ & -70^\circ \leq T_{0,i} \leq 70^\circ (i = 1, 2) \\ & -70^\circ \leq T_{1,i} \leq 70^\circ (i = 1, 2) \\ & n_i = 0, 1, 2, ..., \max(n_i) (i = 1, 2) \\ \text{where:} \quad & \max(n_i) = \begin{cases} \frac{2Lr_s}{\cos(\phi_i)}, \text{if } \phi_i \leq \tan^{-1}\left(\frac{l_x}{l_y}\right) (i = 1, 2) \\ \frac{2Wr_s}{\sin(\phi_i)}, \text{if } \phi_i > \tan^{-1}\left(\frac{l_x}{l_y}\right) (i = 1, 2). \end{cases} \end{aligned} \tag{13}$$

Table 2 Structural Performance of Unholed Optimum Straight Fiber Plate. These values are the targets for the holed straight and fiber-steered structures to achieve in the optimization.

Laminate	Layup	t	m (kg)	$\overline{\overline{E}}_x$ (GPa)	P_{cr} (N)
SF_0	$[\pm 45]_{2s}$	$[t_0]_{2s}$	1.65	0.04	312

Table 3 Structural performance of holed straight fiber plates relative to optimum straight fiber presented in Tab. 2. Solutions from the optimization are presented which achieve the target within ±2%.

Laminate	Layup	t	$m^{\text{Hole}}/m^{\text{ref.}}$	$\overline{E}_x^{\text{Hole}}/\overline{E}_x^{\text{ref.}}$	$P_{\text{cr}}^{\text{Hole}}/P_{\text{cr}}^{\text{ref.}}$
SF_1	$[\pm 64/\pm 46]_s$	$[(1.14t_0)_2/(1.11t_0)_2]_s$	1.05	1.02	0.98
SF_2	$[\pm 75/\pm 52]_s$	$[(1.15t_0)_2/(1.35t_0)_2]_s$	1.17	1.01	1.03
SF_3	$[\pm 79/\pm 54]_s$	$[(1.22t_0)_2/(1.37t_0)_2]_s$	1.21	1.00	1.03

As done previously in Section VI.A for Eqn.11 into Eqn.12 an identical penalty is introduced to reformulate Eqn.13 as

$$\min_x \quad m(x) \cdot (1 + \sqrt{(P_{\text{cr}}^{\text{CTS,Hole}}(x) - P_{\text{cr}}^{\text{ref.}})^2 + (\overline{E}_{x,\text{pre}}^{\text{CTS,Hole}}(x) - \overline{E}_{x,\text{pre}}^{\text{ref.}})^2})^3 \tag{14}$$

VII. Results

The following section presents the results obtained from solving the optimization problems presented in Sections VI.A and VI.B. First Section VII.A presents and discusses the potential for mechanically cloaking a central circular hole in a straight fiber plate by use of traditional straight fiber layups which are free to select ply orientation and thickness. Similarly, in Section VII.B, the results form the fiber-steered optimization problem are presented and discussed. A comparison between mechanical cloaking by straight or fiber steering is made as to begin to uncover the mechanics of the problems.

First, the target unholed optimum straight fiber performance parameters are presented in Tab. 2 where t is an array of ply thicknesses.

A. Straight Fiber Results

The optimization results of the problem presented in Section VI.A are presented in Tab 3. As expected the straight fiber optimization identifies several solutions which achieve within ±2% cloaking of the central hole. By giving the optimizer freedom to select both ply angles (θ_i) and thickness scaling factors (f_i) applied to the nominal ply thickness (t_0) this work proposes several mechanical cloaking solutions by conventional straight fiber design.

Due to the fitness function in Eqn.12 which minimizes mass by application of a penalty to the two-dimensional Euclidean distance, a $[\pm 79/\pm 54]_s$ fiber orientation layup with a thickness layup of $[(1.22t_0)_2/(1.37t_0)_2]_s$ is most optimum in achieving cloaking by merit of lowest fitness function.

This is an extension of a similar analysis to that undertaken by Shin *et al.* [37], where instead of the ply thickness being unconstrained, in this work the optimizer can only select between 1× and 1.5× the nominal ply thickness. Shin *et al.* instead left ply thickness unconstrained which lead to an invariance of buckling load on fiber orientation [37]. Clearly, one can expect that the performance of a certain angle ply laminate to be met by another where the ply thickness is increased such that the target is met. Instead the application of bounds to the potential ply thicknesses as $1 \leq f_i t_0 \leq 1.5$ means that, unlike the work of Shin *et al.*, there are unique ply angle and ply thickness solutions that are most optimal. This is evident with the clustering of optimization results around $75 \leq \theta_1 \leq 79$ and $52 \leq \theta_1 \leq 54$. If the bounds were not applied to the ply thickness then it is simple for the optimizer to meet the target unholed performance by simply increasing the ply thickness to the required value. Thus by comparing performances of SF_0 and SF_3, the holed plate can achieve within a 3% buckling load and effectively identical prebuckling stiffness of the target unholed plate. SF_3 is selected as most optimal as it is that which minimizes the fitness function.

Acceptably the SF_1 and SF_2 solutions are close to the target and indeed are of lower mass than SF_3. However, due to the mass penalty applied to the Euclidean distance of the current and target solutions these lower mass structures are

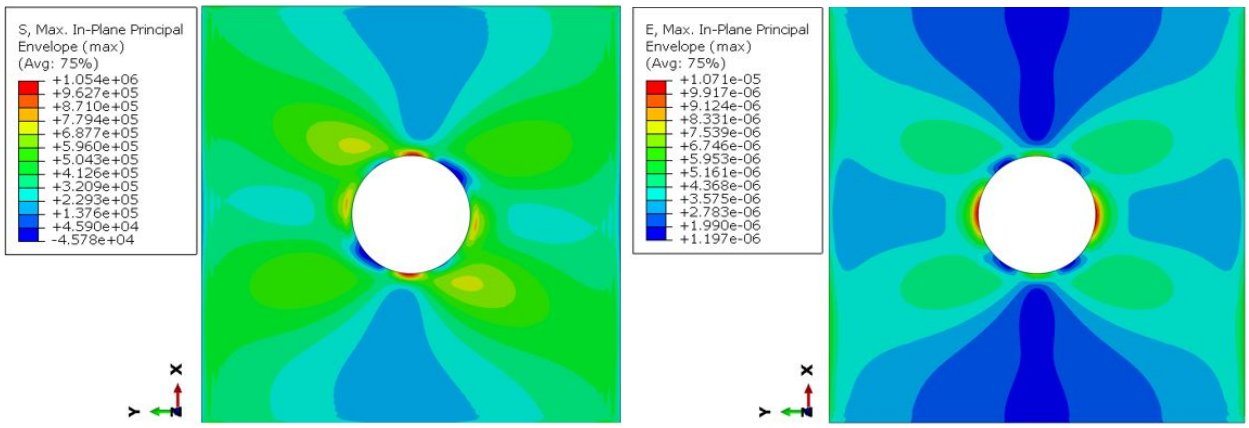

Fig. 5 Maximum in-plane principal (L) stress and (R) strain of target unholed straight fiber plate. Distributions are plotted for mass-optimal mechanical cloaking by straight fiber solution, $[\pm 79/\pm 54]_s$, which achieves target design performance with 21% mass increase. Contours plotted for end shortening equal to linear eigenvalue output ($8.63 \times 10^{-6} m$).

Table 4 Structural performance of holed CTS fiber-steered plates relative to optimum straight fiber presented in Tab. 2. Solutions from the optimization are presented which achieve the target within ±2%.

Laminate	Layup	$m^{\text{Hole}}/m^{\text{ref.}}$	$\overline{E}_x^{\text{Hole}}/\overline{E}_x^{\text{ref.}}$	$P_{cr}^{\text{Hole}}/P_{\text{cr}}^{\text{ref.}}$
CTS_1	$[\pm 45\langle 30\vert 35\rangle^3/\pm 90\langle 38\vert 48\rangle^{10}]_s$	1.19	1.00	0.98
CTS_2	$[\pm 90\langle 34\vert 21\rangle^{10}/\pm 90\langle 52\vert 3\rangle^4]_s$	1.10	1.01	1.01
CTS_3	$[\pm 90\langle 33\vert 21\rangle^{10}/\pm 90\langle 52\vert 2\rangle^4]_s$	1.09	1.01	0.99

penalized due to the prebuckling stiffness and buckling load mismatch. Due to the cubic power selected for the penalty in Eqn.14 even small differences between the target buckling load and prebuckling stiffness are exponentiated. Hence, SF_3 is selected as most optimal and achieves mechanical cloaking of the central hole by employing conventional straight fiber design strategy for a 21% mass increase. Thus, this is where one's engineering judgment would be employed as to determine the sensitivity of the design application to minor mismatches in performance. This investigation considers the problem purely mathematically and thus selects SF_3 as that which is most optimal. Furthermore, as can be inspected in Fig.5, the removal of material at the plate center has significant disruption to both the resulting stress and strain distribution. There are both stress and strain peaks attached to the hole boundary which is as expected for this particular geometrical setup.

B. CTS Fiber-Steered Results

CTS fiber steering achieves structural performance tailoring by generation of periodic fiber angle and thickness distributions on a ply. Where the straight fiber optimization has the freedom to tune ply level constant fiber angles and thicknesses, the CTS fiber steering optimization instead tailors the response by selection of reference path variables, discussed previously in Section I.A as to generate smooth stiffness distributions. Selecting the optimisation bounds on the optimization results dataset as ±2% of target prebuckling stiffness and buckling load, the CTS fiber-steered structural configuration results produced by the optimizer are presented in Tab 4.

As presented, the CTS fiber-steered structural solutions can indeed mechanically cloak the presence of the central circular cutout by generation of periodic stiffness variations, where all configurations presented in Tab. 4 achieve within ±2% performance of the unholed optimized straight fiber target, which has performance as presented previously in Tab. 2. The use of periodic CTS fiber steering generates a non-constant fiber orientation and thickness profile on the plate as traced in Fig.6. One can observe that the first ply $90\langle 33\vert 21\rangle^{10}$ ply of the CTS_3 design has comparatively lower fiber steering than that of the second $\pm 90\langle 52\vert 2\rangle^4$ ply. The $90\langle 33\vert 21\rangle^{10}$ ply is minimally steered and, generally-speaking, aligns the fiber orientations approximately 45° which is most optimal for compression buckling resistance of this particular square plate aspect ratio. Furthermore the steering of the $90\langle 33\vert 21\rangle^{10}$ does generate a small thickness

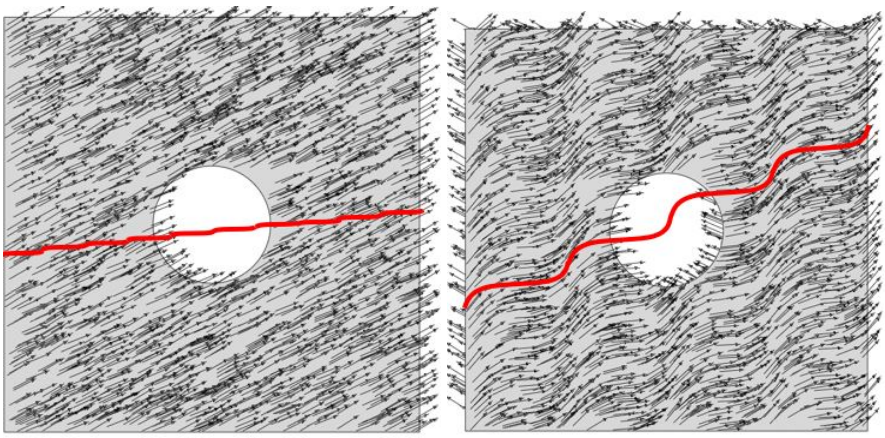

Fig. 6 Tracing the fiber-steered reference path (red) of (L) $90\langle 33|21\rangle^{10}$ and (R) $\pm 90\langle 52|2\rangle^{4}$ plies which feature in design CTS_3. Fiber orientations are extracted from the Finite Element model of the optimal mechanical cloaking by CTS fiber steering configuration.

variation. Due to the non-zero T_0 and T_1 values of this ply the overall thickness will be greater than that if T_0 or T_1 were to equal zero. Consider also the placement of this $90\langle 33|21\rangle^{10}$ in the layup, it corresponds to those at the largest distance from the neutral axis and thus compounds the orientation and thickness benefits in terms of flexural stiffness. The $\pm 90\langle 52|2\rangle^{4}$ ply acts akin to a hybrid between that seen in the literature and conventional stiffened panel design. The high difference between T_0 and T_1 acts to promote load redistribution. One will note that the T_0 selection of 52° when once summed with the $\phi = 90°$ steering direction gives a 45° local fiber angle, which is, again the optimal fiber orientation for uniaxial compression buckling of this plate aspect ratio. Furthermore, this local, approximately, 45° orientation is that at which thickness is maximized. The $T_1 = 2°$ aligns fibers perpendicular to the loading direction. This fits the working theory of fiber steering whereby load is redistributed from angles perpendicular to the load towards ones more aligned. If the plate's performance was to be maximized then ideally, T_0 would be aligned to the loading direction as to fully exploit mechanical load redistribution. However, the objective of the optimization is to match a target performance and not exceed it, and further alignment of the fiber orientation with the loading direction would incur a Euclidean distance penalty and never be selected by the GA if encountered within a particular population pool. Figure 8 presents the resulting thickness build-up pattern of CTS_3 where it is evident that the more aggressive steering of the $\pm 90\langle 52|2\rangle^{4}$ plies compared to the $90\langle 33|21\rangle^{10}$ leads to 4 dominant thickness build-ups. Moreover, upon inspection of Fig.8 it is evident that the optimal selection of $\phi = 90$ is clear as to align the thickness build-ups to the loading direction, which helps to concentrate compression loads in the thicker regions (load follows stiffness) and thereby steer them away from the cutout.

Furthermore, Fig.7 presents the resulting maximum in-plane principal stress and strain of CTS_3. As can be inspected both stress and strain distributions are highly non-uniform due to: (1) the presence of the central hole, such as that seen previously in Fig. 5; and (2) the effects of periodic CTS fiber steering generating non-constant material stiffness. However, there does seem to be a regularity to the distributions. If the analogy of 'pseudo-stiffeners' proposed by Lincoln *et al.* [30] is employed here, the thicker regions are acting as such pseudo-stiffeners, thereby attracting load. Furthermore, the thicker regions occur at the period center, due to $T_0 > T_1$, and as such there are thicker regions conveniently placed at the supported plate edges. The location of these thicker, and consequently, higher stiffness regions at the panel edges acts to reinforce the simply-supported boundary conditions. Reinforcement of the boundary conditions is what Hyer and Lee [5] hypothesized in their initial work where, if the load paths can be redirected to the supports, then improved structural performance can be obtained. It is interesting that the thickness build-up at the mid-plate intersects the hole. In common stringer reinforced panel design the hole would be entrapped in a stiffener bay. Instead due to the optimizer selected periodicity of the reference path, and the hole size it is not possible to entrap the hole between two thickness build-ups. The distance between thickness build-ups, analogous to stringer pitch, does not allow confinement of the hole between maxima.

Furthermore, upon inspection of Fig.10 one can observe the beneficial phenomena at work in the design of CTS_3 over ST_3. The colormaps of Fig.7 are queried to extract raw data along the magenta line denoted in Fig. 8. As Fig. 7 denotes there is detachment of the stress and strain peaks away from the hole towards the thickness build-ups. Comparing

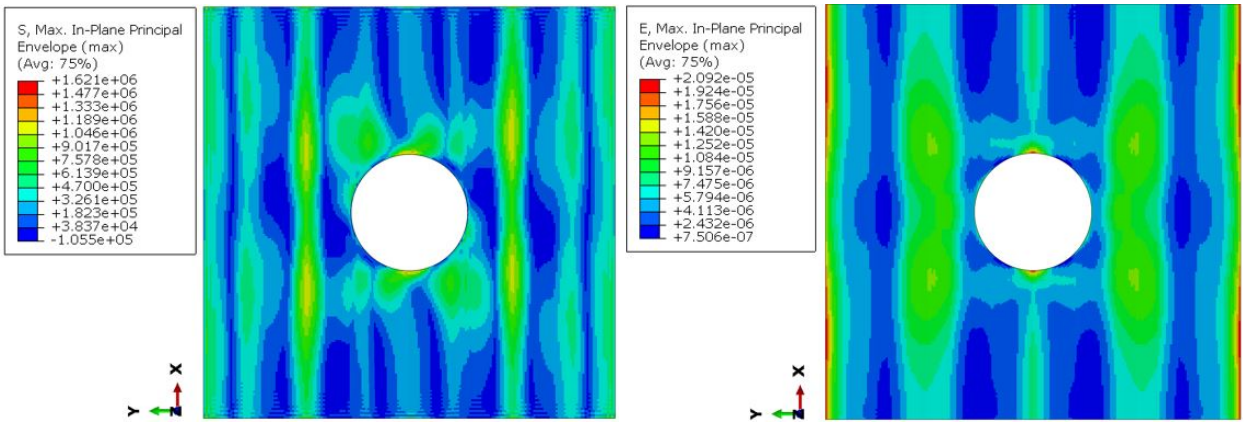

Fig. 7 Maximum in-plane principal (L) stress and (R) strain of target unholed straight fiber plate. Distributions are plotted for optimal mechanical cloaking by fiber-steered solution, $[\pm 90\langle 33|21\rangle^{10}/\pm 90\langle 52|2\rangle^{4}]_s$, which achieves target design performance with 9% mass increase. Note the significant loading redistribution by CTS fiber steering and the action of the thicker, higher stiffness regions as 'pseduo-stiffeners'. Again, contours plotted for end shortening equal to linear eigenvalue output ($1.14 \times 10^{-5} m$).

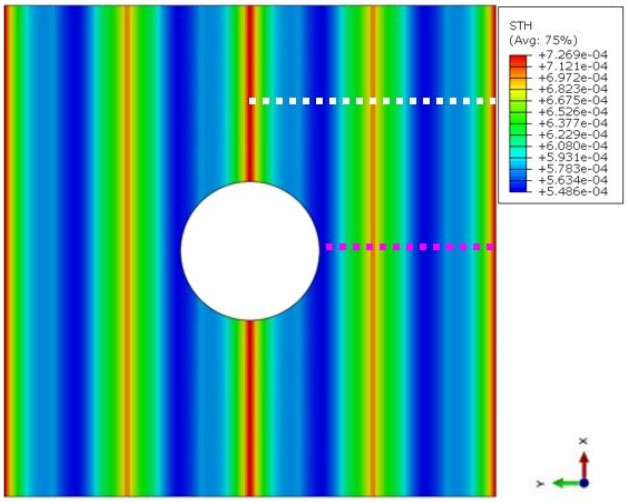

Fig. 8 Resulting thickness profile of $[\pm 90\langle 33|21\rangle^{10}/\pm 90\langle 52|2\rangle^{4}]_s$ due to periodic ply-level CTS fiber steering. Note there are 4 regions of high thickness due to the higher periodic fiber angle difference in interior plies 3 to 6 than those at the outside of the layup.

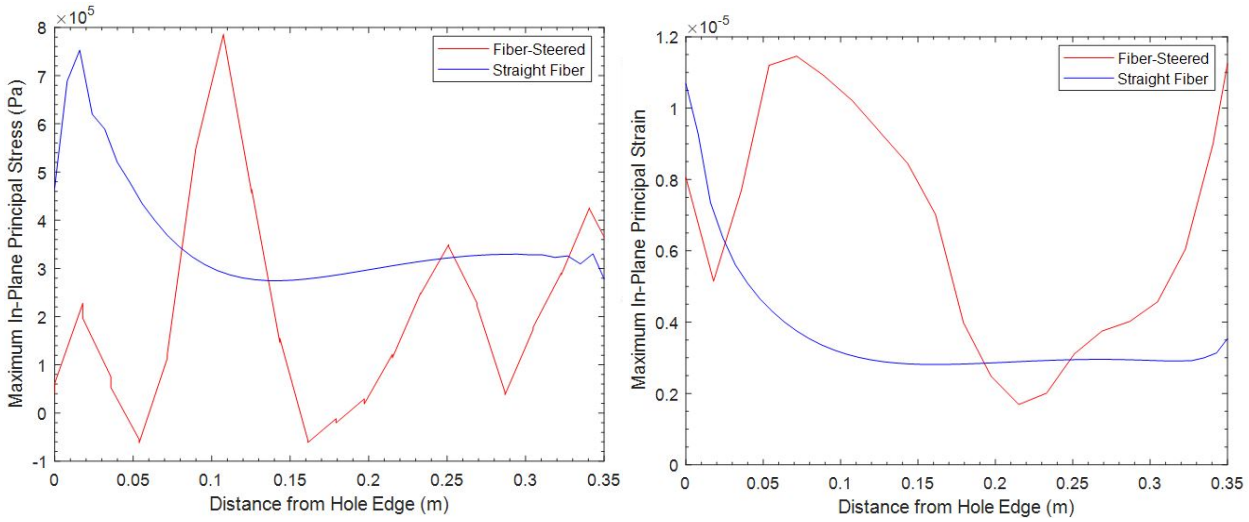

Fig. 9 Extraction of maximum in-plane principal (L) stress and (R) strain of optimal straight and fiber-steered design solutions. Note the alignment of the stress with the pseudo-stiffeners of CTS_3. Note extraction is conducted along the mid-length dashed magenta line of Fig.8

the relative positions of the stress and strain maxima in Fig. 7 one can observe such detachment. As can be seen the fiber-steered solution of CTS_3 is highly nonuniform and a majority of the compressive stress is being redirected away from the hole towards the thicker regions. Furthermore, a majority of the material in the fiber-steered design is less stressed than that of the straight fiber structure. Hence, partial detachment of the critical stress component from the hole by means of fiber steering is an efficient structural design tactic to tailor structural performance. In addition to the 2 dominant stress peaks, corresponding to the thickness maxima of the $\pm 90\langle 52|2\rangle^4$ plies, there is 1 between them which corresponds instead to the minor thickness maxima from the $90\langle 33|21\rangle^{10}$ plies being interspersed between the dominant maxima. Hence, this interspersing acts to redistribute load in between the $\pm 90\langle 52|2\rangle^4$ dominant thickness maxima.

Finally a comparison between the linearized prebuckling response of all proposed solutions and the target structure is presented in Fig. 11. Where one can inspect how close each solution is to the target. Note the 3D plot gives an additional axis to account for the relative mass increase of all presented solutions to mechanically cloak the presence of the central hole.

VIII. Conclusion

In conclusion, mechanical cloaking, the potential of a holed structure to have equal performance to that of an unholed structure is achievable, and by doing so at lowest possible mass increase is what is most pertinent for future aerospace design. The use of advanced fiber-reinforced composite material systems provides a designer with significant freedom to tailor the structural response to meet strict performance criteria, as has been done herein. Furthermore, the extension of fiber-reinforced materials from straight to fiber-steered represents a remarkable expansion of the current design space available. This work has indeed broadened the existing design space of fiber-reinforced plate structures by optimizing fiber-steered configurations. In regards to achieving mechanical cloaking of a square, $l_x/l_y = 1.0$, simply supported panel with central cutout $D/W = 0.3$, a straight fiber layup is proposed that tailors both ply level fiber orientation and ply thickness to achieve mechanical cloaking within 2% for a 21% performance increase. Comparatively, a CTS fiber-steered panel is proposed which achieves mechanical cloaking within 1% for a 9% mass increase. It is of note that this investigation has only considered the solution space of $\phi = [0, \pm 45, 90]$, clearly there is a sufficiently large solution space in that steering direction can have any value in $0° \leq \phi \leq 90°$. The novelty in this work is in the expansion of the common design space to consider periodic fiber steering of a ply. This periodic fiber steering extends and combines prior literature hypotheses, namely load redistribution towards supported edges of Hyer and Lee [6] and the more recent pseudo-stiffener hypothesis of Lincoln *et al.* [30]. Future work aims to identify and examine the potential sources of nonlinearities that reside in CTS fiber-steered plate design and their effect on the designs proposed in this current work.

In summation fiber steering by the CTS process represents a significant potential for structural performance tailoring

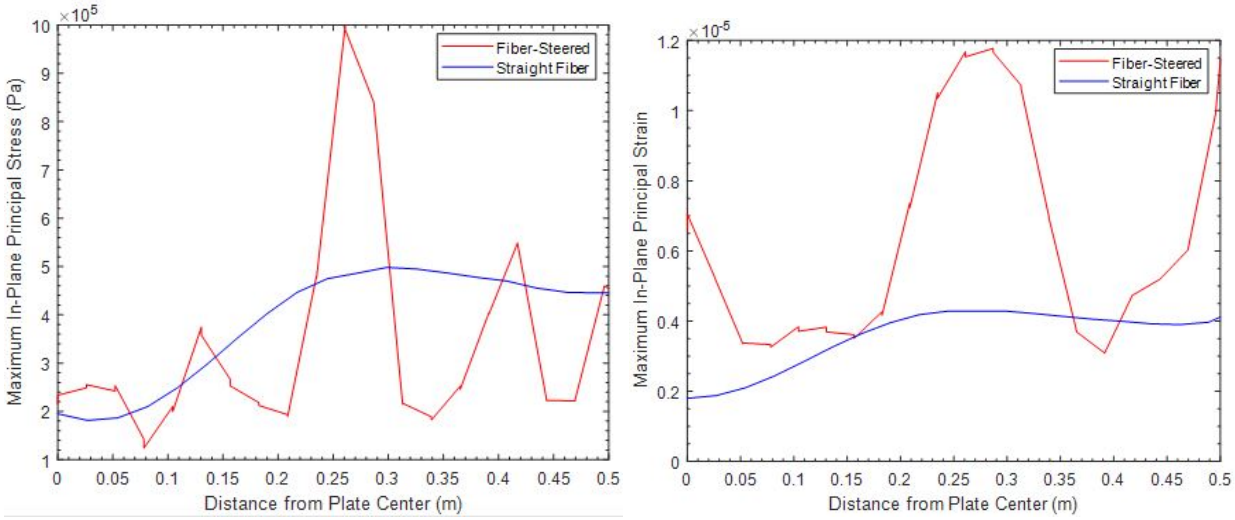

Fig. 10 Extraction of maximum in-plane principal (L) stress and (R) strain of optimal straight and fiber-steered design solutions. Note the alignment of the stress with the pseudo-stiffeners of CTS_3. Note extraction is conducted along the three quarter length dashed white line of Fig.8

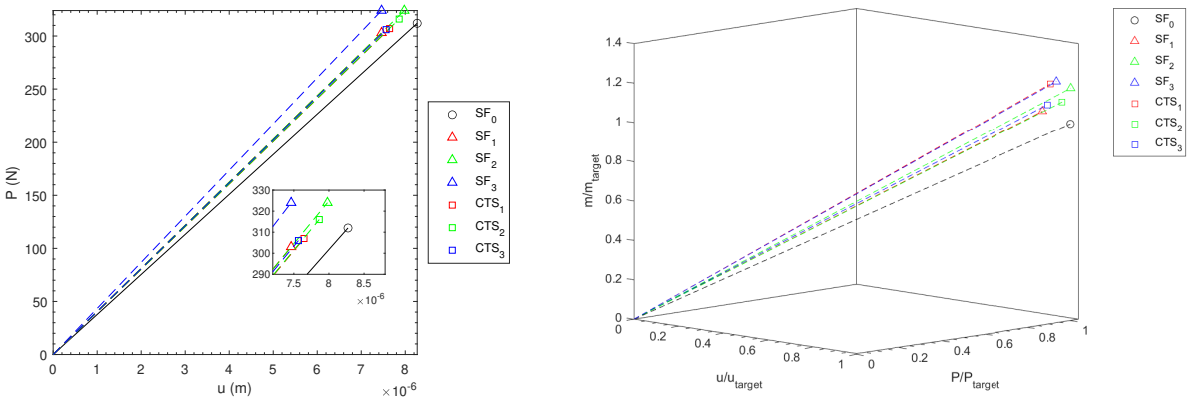

Fig. 11 Linearized buckling performance of all proposed holed straight and fiber-steered plates with reference to an unholed target plate.

through design of variable-angle, variable-thickness structures. Overall, the now expanded design space is sufficiently rich and clearly requires significant effort to utilize in efficient structural design. However, as has been discussed herein the mechanics arising are often non-intuitive and require careful consideration and analysis for application to future aerostructural research and development.

Acknowledgments

This work was supported by the Engineering and Physical Sciences Research Council through the EPSRC Centre for Doctoral Training in Composites Science, Engineering and Manufacturing [grant number EP/S021728/1]. R.M.J. Groh acknowledges the support of the Royal Academy of Engineering under the Research Fellowship scheme [Grant No. RF\201718\17178]. This work was carried out using the computational facilities of the Advanced Computing Research Center, University of Bristol - http://www.bris.ac.uk/acrc/.

References

[1] Chow, F.-y., and Rangachari, N., "Buckling of Plates Containing Openings," *7th International Specialty Conference on Cold-Formed Steel Structures*, (St. Louis, 1984, pp. 39–54.

[2] Turvey, G., and Marshall, I., *Buckling and Postbuckling of Composite Plates*, 1st ed., Capman & Hall, Londom, 1995.

[3] Nemeth, M. P., "Buckling and postbuckling behaviour of laminated composite plates with a cut-out," *Buckling and Postbuckling of Composite Plates*, , No. July 1996, 1995, pp. 260–298. https://doi.org/10.1007/978-94-011-1228-4{_}8.

[4] Lee, H. H., and Hyer, M. W., "Postbuckling failure of composite plates with holes," *AIAA Journal*, Vol. 31, No. 7, 1993, pp. 1293–1298. https://doi.org/10.2514/3.11766.

[5] Hyer, M. W., and Charette, R. F., "Use of curvilinear fiber format in composite structure design," *AIAA Journal*, Vol. 29, No. 6, 1991, pp. 1011–1015. https://doi.org/10.2514/3.10697.

[6] Hyer, M. W., and Lee, H. H., "The use of curvilinear fiber format to improve buckling resistance of composite plates with central circular holes," *Composite Structures*, Vol. 18, No. 3, 1991, pp. 239–261. https://doi.org/10.1016/0263-8223(91)90035-W.

[7] Jegley, D. C., Tatting, B. F., and Gürdal, Z., "Tow-steered panels with holes subjected to compression or shear loading," *Collection of Technical Papers - AIAA/ASME/ASCE/AHS/ASC Structures, Structural Dynamics and Materials Conference*, Vol. 5, 2005, pp. 3453–3466. https://doi.org/10.2514/6.2005-2081.

[8] Lopes, C. S., Gürdal, Z., and Camanho, P. P., "Tailoring for strength of composite steered-fibre panels with cutouts," *Composites Part A*, Vol. 41, No. 12, 2010, pp. 1760–1767. https://doi.org/10.1016/j.compositesa.2010.08.011, URL http://dx.doi.org/10.1016/j.compositesa.2010.08.011.

[9] Gürdal, Z., Tatting, B. F., and Wu, C. K., "Variable stiffness composite panels: Effects of stiffness variation on the in-plane and buckling response," *Composites Part A: Applied Science and Manufacturing*, Vol. 39, No. 5, 2008, pp. 911–922. https://doi.org/10.1016/j.compositesa.2007.11.015.

[10] Zucco, G., Rouhi, M., and Oliveri, V., "Continuous Tow Steering Around an Elliptical Cutout in a Composite Panel," *AIAA Journal*, Vol. 59, No. 12, 2021. https://doi.org/10.2514/1.J060668.

[11] Hu, M., Briggert, A., and Olsson, A., "Growth layer and fibre orientation around knots in Norway spruce : a laboratory investigation," 2018, pp. 7–27. https://doi.org/10.1007/s00226-017-0952-3.

[12] Grenoble, R. W., Nguyen, T., McKenney, M. J., Przekop, A., Juarez, P. D., Gregory, E. D., Jegley, D. C., and Oremont, L., "Fabrication of a composite tow-steered structure for air-launch vehicle applications," *AIAA/ASCE/AHS/ASC Structures, Structural Dynamics, and Materials Conference, 2018*, , No. 210049, 2018, pp. 1–14. https://doi.org/10.2514/6.2018-1376.

[13] Heinecke, F., and Willberg, C., "Manufacturing-Induced Imperfections in Composite Parts Manufactured via Automated Fiber Placement," *Journal of Composites Science*, Vol. 3, No. 2, 2019, p. 56. https://doi.org/10.3390/jcs3020056.

[14] Kim, B. C., Potter, K., and Weaver, P. M., "Continuous tow shearing for manufacturing variable angle tow composites," *Composites Part A: Applied Science and Manufacturing*, Vol. 43, No. 8, 2012, pp. 1347–1356. https://doi.org/10.1016/j.compositesa.2012.02.024, URL http://dx.doi.org/10.1016/j.compositesa.2012.02.024.

[15] Matveev, M. Y., Schubel, P. J., Long, A. C., and Jones, I. A., "Understanding the buckling behaviour of steered tows in Automated Dry Fibre Placement (ADFP)," *Composites Part A: Applied Science and Manufacturing*, Vol. 90, 2016, pp. 451–456. https://doi.org/10.1016/j.compositesa.2016.08.014, URL http://dx.doi.org/10.1016/j.compositesa.2016.08.014.

[16] Li, X., Hallett, S. R., and Wisnom, M. R., "Modelling the effect of gaps and overlaps in automated fibre placement (AFP)-manufactured laminates," *Science and Engineering of Composite Materials*, Vol. 22, No. 2, 2015, pp. 115–129. https://doi.org/10.1515/secm-2013-0322.

[17] McInnes, C. J., Lincoln, R. L., Pirrera, A., Kim, B. C., and Groh, R. M., "On the Finite Element Discretization of Continuous Tow-Sheared Structures," *AIAA Science and Technology Forum and Exposition, AIAA SciTech Forum 2022*, 2022, pp. 1–19. https://doi.org/10.2514/6.2022-2598.

[18] Kim, B. C., Weaver, P. M., and Potter, K., "Computer aided modelling of variable angle tow composites manufactured by continuous tow shearing," *Composite Structures*, Vol. 129, 2015, pp. 256–267. https://doi.org/10.1016/j.compstruct.2015.04.012, URL http://dx.doi.org/10.1016/j.compstruct.2015.04.012.

[19] Groh, R. M., and Weaver, P. M., "Mass optimization of variable angle tow, variable thickness panels with static failure and buckling constraints," *56th AIAA/ASCE/AHS/ASC Structures, Structural Dynamics, and Materials Conference*, , No. January, 2015. https://doi.org/10.2514/6.2015-0452.

[20] Gürdal, Z., and Olmedo, R., "In-plane response of laminates with spatially varying fiber orientations: Variable stiffness concept," *AIAA Journal*, Vol. 31, No. 4, 1993, pp. 751–758. https://doi.org/10.2514/3.11613.

[21] Wang, L., Boddapati, J., Liu, K., Zhu, P., Daraio, C., and Chen, W., "Mechanical cloak via data-driven aperiodic metamaterial design," *Proceedings of the National Academy of Sciences of the United States of America*, Vol. 119, No. 13, 2022, pp. 1–8. https://doi.org/10.1073/pnas.2122185119.

[22] Fachinotti, V. D., Peralta, I., and Albanesi, A. E., "Optimization-based design of an elastostatic cloaking device," *Scientific Reports*, Vol. 8, No. 1, 2018, pp. 1–9. https://doi.org/10.1038/s41598-018-28069-7.

[23] Bückmann, T., Kadic, M., Schittny, R., and Wegener, M., "Mechanical cloak design by direct lattice transformation," *Proceedings of the National Academy of Sciences of the United States of America*, Vol. 112, No. 16, 2015, pp. 4930–4934. https://doi.org/10.1073/pnas.1501240112.

[24] Tatting, B. F., and Gurdal, Z., "Design and Manufacture Tow Placed Plates of Elastically Tailored," *NTRS - NASA Technical Reports*, , No. August, 2020. URL https://ntrs.nasa.gov/citations/20020073162.

[25] Stein, M., "National Aeronautics and Loads and Deformations of Buckled Rectangular Plates," *National Aeronautics and Space Administration*, Vol. Technical, 1959.

[26] Chandra, R., and Basava, B., "POSTBUCKLING ANALYSIS OF RECTANGULAR ORTHOTROPIC PLATES," Vol. 15, 1978, pp. 81–97.

[27] White, S. C., "Post-buckling of variable-stiffness shell structures," Ph.D. thesis, University of Bristol, 2017. https://doi.org/10.13140/RG.2.2.28861.46560.

[28] Weaver, P. M., and Nemeth, M. P., "Bounds on Flexural Properties and Buckling Response for Symmetrically Laminated Plate," *Journal of Engineering Mechanics*, Vol. 133, No. 200, 1967, p. 1178.

[29] Nettles, A. T., "Basic Mechanics of Laminated Composite Plates," *NASA reference pulication*, , No. October, 1994, p. 107. URL http://www.ntrs.nasa.gov/archive/nasa/casi.ntrs.nasa.gov/19950009349_1995109349.pdf.

[30] Lincoln, R. L., Weaver, P. M., Pirrera, A., and Groh, R. M., "Imperfection-insensitive continuous tow-sheared cylinders," *Composite Structures*, Vol. 260, 2021, p. 113445. https://doi.org/10.1016/j.compstruct.2020.113445, URL https://doi.org/10.1016/j.compstruct.2020.113445.

[31] Lincoln, R. L., Weaver, P. M., Pirrera, A., and Groh, R. M., "Optimization of imperfection-insensitive continuous tow sheared rocket launch structures," *AIAA Scitech 2021 Forum*, 2021, pp. 1–19. https://doi.org/10.2514/6.2021-0202.

[32] Groh, R. M., and Weaver, P. M., "Mass optimization of variable angle tow, variable thickness panels with static failure and buckling constraints," *56th AIAA/ASCE/AHS/ASC Structures, Structural Dynamics, and Materials Conference*, , No. January, 2015. https://doi.org/10.2514/6.2015-0452.

[33] Dodwell, T. J., Kingdom, U., Butler, R., Rhead, A. T., and Kingdom, U., "Optimum Fiber Steering of Composite Plates for Buckling and Manufacturability," *AIAA Journal*, Vol. 54, No. 3, 2016, pp. 1139–1142. https://doi.org/10.2514/1.J054297.

[34] Dassault Systèmes Simulia Corp., *Abaqus User's Manual*, 6th ed., Dassault Systèmes, Providence, 2021.

[35] MathWorks, "MATLAB (Version 2021b)," , 2021.

[36] McCall, J., "Genetic algorithms for modelling and optimisation," *Journal of Computational and Applied Mathematics*, Vol. 184, No. 1, 2005, pp. 205–222. https://doi.org/10.1016/j.cam.2004.07.034.

[37] Shin, Y. S., Haftka, R. T., Watson, L. T., and Plaut, R. H., "Design of Laminated Plates for Maximum Buckling Load," *Journal of Composite Materials*, Vol. 23, No. 4, 1988, pp. 348–369.